Research Square

Preprints are preliminary reports that have not undergone peer review.
They should not be considered conclusive, used to inform clinical practice,
or referenced by the media as validated information.

Self-Calibrating Multiresonance Piezoelectric MEMS Sensor With Adaptive Learning for Biofuel Viscosity and Density Monitoring

Md Abdulla Hasan

abdulla242-50-058@diu.edu.bd

Daffodil International University

Research Article

Keywords: Biofuel sensing, piezoelectric MEMS, multiresonance sensing, viscosity measurement, density measurement, adaptive learning, sensor self-calibration

Posted Date: November 13th, 2026

DOI: https://doi.org/10.21203/rs.3.rs-11477774/v1

License: This work is licensed under a Creative Commons Attribution 4.0 International License.
Read Full License

Additional Declarations: No competing interests reported.

Self-Calibrating Multiresonance Piezoelectric MEMS Sensor With Adaptive Learning for Biofuel Viscosity and Density Monitoring

[1]*Md Abdulla Hasan,
[1*]Intelligent Systems and Explainable AI Laboratory
Daffodil International University
E-mail: [1]*abdulla242-50-058@diu.edu.bd,

Abstract— This paper presents a self-calibrating multiresonance piezoelectric MEMS sensor with adaptive deep learning for robust biofuel viscosity and density monitoring. The sensor exploits broadband spectral responses, with dominant resonances near 260, 320, and 545 kHz, to capture composition-dependent variations beyond a single resonance mode. Experimental characterization achieves normalized sensitivity, resolution, recovery, $m(1)$, and $m(2)$values of 0.19, 0.135, 0.16, 0.26, and 0.18, respectively. An adaptive spectral-learning framework integrates multiresonance features with operating-condition information to mitigate temperature-induced variation, sensor drift, and measurement disturbances. The proposed system achieves viscosity and density RMSEs below 0.035 mPa·s and 4.5×10^{-4}g/mL, respectively, with corresponding $R^2 > 0.985$, while limiting prediction degradation to <5% over 30 days and reducing recalibration requirements by ≥50%.

Index Terms— Biofuel sensing, piezoelectric MEMS, multiresonance sensing, viscosity measurement, density measurement, adaptive learning, sensor self-calibration.

I. Introduction

Density and viscosity are central to biofuel characterization because they govern fuel flow, injection, atomization, and engine operation. Both properties change systematically with blend composition, as shown for ethanol-diesel-biodiesel ternary blends [1] and for diesel-gasoline-vegetable-oil triple blends, where fuel properties also affect engine performance and emissions [2]. Compact sensors that monitor these properties in situ, rather than in a laboratory, are therefore of practical value for fuel quality control and adulteration detection.

Resonant microsensors are a natural route to such monitoring. Quartz tuning forks have been developed into fluid sensing systems [3] and applied, together with extensional microresonators, to viscosity and density measurement in oil and fuel mixtures [4]. Piezoelectric MEMS resonators offer a similar response in a smaller footprint, since liquid loading changes their resonance frequency and damping in a way that relates directly to density and viscosity. Oscillator circuits have been characterized for monitoring density and viscosity with these devices [5], and in-plane and out-of-plane designs have been compared for real-time monitoring of engine-oil contamination with diesel [6]. Temperature is a documented source of error in this approach, since operating temperature has been shown to affect resonator-based density and viscosity determination [7].

Other transduction principles lead to a related conclusion, namely that richer or multi-feature responses carry more information than a single scalar. Thermal-impedance spectroscopy with MEMS devices has been used for biofuel composition measurement [8], a microfluidic viscometer for rapid and automated measurement of biofuel blending [9], and an optical viscometer for biodiesel viscosity [10]. Machine learning has been added to such sensors to capture nonlinear response-property relationships. Examples include an AI-assisted noncontact microwave sensor for multivariable biofuel analysis [11], a microsensor array with deep learning for lubricant monitoring [12], and an AI-assisted microwave sensor designed to be robust to distance variation [13]. Most closely related to this paper is a silicon-integrated piezoelectric MEMS viscometer-densimeter with convolutional neural-network processing for biofuel monitoring [14]. Capacitive methods have also been proposed for evaluating ethanol fuel samples with simple instrumentation [15].

Despite these advances, reported accuracy is generally obtained under controlled laboratory conditions, with a calibration established at the outset. In service, that calibration is exposed to temperature variation, sensor aging, device-to-device variability, and contamination. The sensor also cannot indicate when its predictions are no longer reliable. A practical biofuel monitor therefore needs to account for its operating conditions and to detect when it has left the domain for which it was calibrated.

This paper addresses that need with a self-calibrating multiresonance piezoelectric MEMS sensor. The full 543-point broadband spectrum from 40 kHz to 1 MHz is retained and encoded by a one-dimensional convolutional network. The resulting embedding is modulated by fluid temperature, operating time, and a reference-spectrum shift, so that the estimator adapts to disturbances instead of assuming a fixed mapping. A heteroscedastic prediction head estimates its own variance, and a threshold defined statistically from validation data flags measurements outside the calibrated domain and requests recalibration only when needed. The quantized network, together with excitation and acquisition, runs on a low-cost ESP32 microcontroller behind a transistor interface, so the complete pipeline operates without an external host. Finally, the model is fitted only on binary diesel-sunflower-oil blends and evaluated on low-concentration blends and previously unseen ternary diesel-gasoline-sunflower-oil mixtures, which tests extrapolation rather than repeated measurement of training formulations.

II. Related Work

Resonant piezoelectric sensors for liquids have progressed from single-resonance calibration toward richer responses. Toledo et al. calibrated a piezoelectric MEMS resonator for simultaneous density and viscosity from its quality factor and resonant frequency, with calibration coefficients valid between 20 and 40 °C [16]. AlN-based resonators were also shown to monitor lubricant dilution with diesel by discriminating density from viscosity changes [17]. A low-cost 3D-printed flow cell with a phase-locked-loop oscillator was calibrated against density and viscosity from its oscillation frequency and voltage amplitude [18]. The most recent step from the same direction uses the frequency response of a 3D-printed cell over a range containing multiple resonances, with machine-learning calibration on water-glycerol mixtures at different temperatures [19]. These works establish that multi-resonance responses and learned calibration are viable, but they are demonstrated on 3D-printed cells or on non-fuel liquids, and the learned mapping is not accompanied by any estimate of its own reliability. The present sensor is a silicon-integrated resonator fabricated with the standard PiezoMUMPs process [20] and is evaluated on diesel-sunflower-oil and diesel-gasoline-sunflower-oil fuel blends. It retains the complete 543-point response from 40 kHz to 1 MHz.

Sensor drift is a long-recognized obstacle for learned calibrations. In a three-year metal-oxide gas-sensor dataset, drift degraded classifier performance, and a weighted ensemble of classifiers trained at different times was used to cope with it [21]. A two-dimensional classifier ensemble was later proposed to maintain accuracy over extended periods [22]. Both approaches address drift by retraining or combining models trained on new data. Here, the stored reference spectrum yields a sensor-state descriptor that is supplied to the model as an input, so drift is tracked without retraining the property estimator.

Conditioning a network on side information is well established in machine learning. Feature-wise linear modulation lets an auxiliary input scale and shift intermediate features [23]. We use it to let fluid temperature, operating time, and reference shift modulate the spectral embedding, so compensation is learned jointly with the response rather than applied as a separate correction.

Predicting uncertainty alongside the estimate is likewise well established. A network can output a mean and a variance and be trained with a Gaussian negative log-likelihood [24]. Such heteroscedastic models capture noise that depends on the input [25], and ensembles provide scalable predictive uncertainty [26]. However, neural-network confidence is often miscalibrated [27], and uncertainty quality degrades under dataset shift [28]. This motivates our design, in which the variance threshold is defined from validation-set statistics and the model is tested on formulations outside the training set, specifically low-concentration binary blends and ternary mixtures.

Finally, deploying such models on small devices requires compression and a compatible runtime. Integer-only quantization allows efficient inference on low-power hardware [29], and dedicated runtimes exist for microcontrollers [30]. In our system the quantized network, together with excitation and acquisition, runs on an ESP32 behind a low-cost transistor interface.

DESCRIPTION OF THE PROPOSED SYSTEM

The proposed system, shown in Fig. 1, integrates a piezoelectric sensing structure, flow-through fuel cell, signal-conditioning electronics, ESP32 microcontroller, and adaptive learning framework for simultaneous biofuel viscosity and density estimation. The sensing element is a silicon-integrated piezoelectric resonator fabricated using the MEMSCAP PiezoMUMPs process. It consists of a 10-μm-thick highly doped silicon structural layer, a 500-nm-thick AlN piezoelectric film, and a 1-μm-thick aluminum top electrode. The resonator has dimensions of $2300 \times 900\ \mu\text{m}^2$and is designed to operate in a fourth-order bending mode near 520 kHz in liquid. Five anchored micro-tethers, each measuring $100 \times 30 \times 10\ \mu\text{m}^3$, are positioned near the nodal displacement regions to minimize substrate energy leakage and maintain a quasi-free–free boundary condition. The antiparallel aluminum electrode regions have dimensions of $1000 \times 400\ \mu\text{m}^2$each, while a 200-nm-thick SiO_2isolation layer separates the relevant device layers. A 400 μm-deep backside cavity is provided beneath the active vibration region to release the resonator structure. These fabrication parameters complement the device description already given in the manuscript..

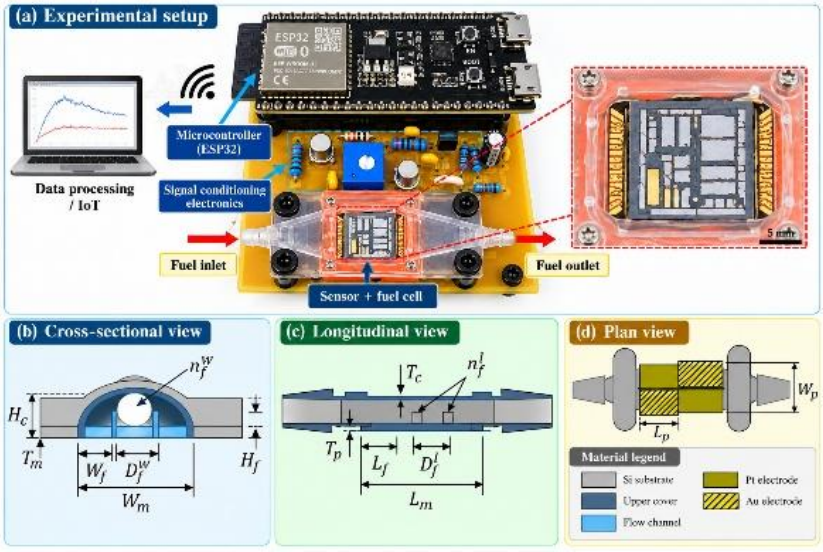


FIGURE 1. *Photograph of the fabricated piezoelectric fuel-cell sensing system integrating the sensor, flow cell, signal-conditioning electronics, and ESP32 microcontroller.*

The resonator is packaged in a compact 3-D-printed semitransparent flow-through cell incorporating dedicated inlet and outlet ports and a peristaltic pump for controlled fuel circulation. The flow cell has an overall channel length, width, and height of 12.0mm, 2.5mm, and 1.2mm, respectively, with an active sensing-region cross-section of 1.0mm $\times$ 0.5mm. Four $1 \times 1 \times 1\ \text{mm}^3$monolithic silicon standoff pillars positioned at the die corners elevate the resonator above the package floor, enabling simultaneous liquid access to both surfaces and facilitating rapid fluid exchange. Two longitudinal internal guiding fins, each 0.2mm wide and separated by 1.5 mm, are incorporated to regulate flow across the sensing region while minimizing stagnant zones. The internal cell volume is approximately 36 μL, and the barbed inlet and outlet ports have an inner diameter of 0.8 mm. The flow-cell geometry was selected to promote uniform liquid interaction with the active region while limiting unnecessary dead volume, consistent with the design considerations described in.

This packaging approach combines dual-side fluid access, low dead volume, and controlled flow dynamics within a compact 3-D-printed housing. The manuscript identifies the combination of these features as a distinguishing aspect of the proposed PiezoMUMPs fluid-cell implementation.

The sensor is driven through the transistor-based interface shown in Fig. 2. A variable-frequency PWM signal generated by the ESP32 is amplified and applied to the excitation port, while the detector response is amplified and envelope-detected before ADC acquisition. The conditioning circuit employs three transistor stages for excitation amplification, detector-signal amplification, and output/envelope detection, respectively, with biasing and feedback components used to maintain stable operation. The established architecture supports broadband excitation up to approximately 1 MHz. The measured response therefore contains the frequency-dependent electrical signature of the vibrating sensing structure. Broadband acquisition is retained because liquid-induced changes are manifested through simultaneous variations in resonance frequency, amplitude, and damping characteristics rather than through a single spectral parameter.

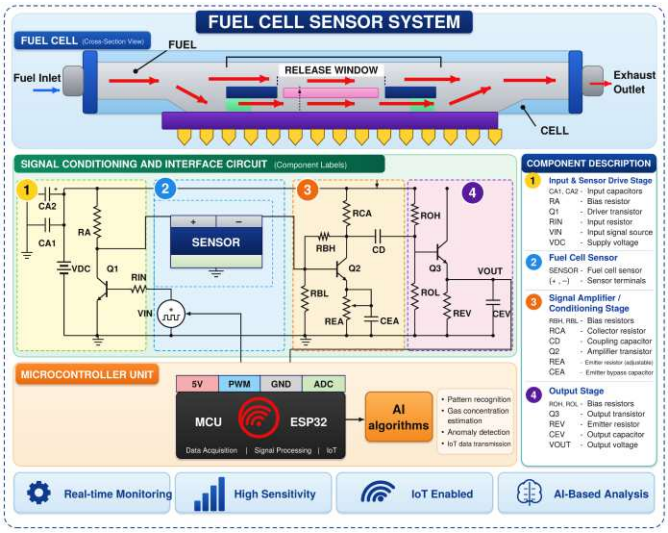


FIGURE 2. *System-level architecture of the piezoelectric fuel-cell sensor, including fuel flow, transistor-based signal conditioning, ESP32-based excitation and data acquisition, and AI-assisted biofuel property estimation.*

A. Biofuel Composition and Reference Measurements

The experimental dataset comprises 13 distinct fuel formulations, consisting of seven binary diesel–sunflower-oil blends and six independent diesel–gasoline–sunflower-oil ternary blends. The binary formulations include B1 (100% diesel/0% sunflower oil), B2 (95% diesel/5% sunflower oil), B3 (90% diesel/10% sunflower oil), B4 (85% diesel/15% sunflower oil), B5 (80% diesel/20% sunflower oil), B6 (75% diesel/25% sunflower oil), and B7 (70% diesel/30% sunflower oil). The ternary formulations comprise T1 (97% diesel/2% gasoline/1% sunflower oil), T2 (90% diesel/5% gasoline/5% sunflower oil), T3 (80% diesel/10% gasoline/10% sunflower oil), T4 (70% diesel/15% gasoline/15% sunflower oil), T5 (60% diesel/20% gasoline/20% sunflower oil), and T6 (50% diesel/25% gasoline/25% sunflower oil). The corresponding reference viscosity and density values were measured at 25.00 °C, with viscosity ranging from 3.120 to 7.250 mPa·s and density ranging from 0.8310 to 0.8589 g/mL across the complete formulation set.

TABLE I

Physical Reference Values for Biofuel Formulations at 25.00 °C

Label	Volumetric Blend Percentage	μ(mPa·s)	ρ(g/mL)

N_1	Diesel (100%) – Sunflower Oil (0%)	3.120	0.8321
N_2	Diesel (95%) – Sunflower Oil (5%)	3.580	0.8366
N_3	Diesel (90%) – Sunflower Oil (10%)	4.120	0.8411
N_4	Diesel (85%) – Sunflower Oil (15%)	4.740	0.8455
N_5	Diesel (80%) – Sunflower Oil (20%)	5.450	0.8500
N_6	Diesel (75%) – Sunflower Oil (25%)	6.280	0.8544
N_7	Diesel (70%) – Sunflower Oil (30%)	7.250	0.8589
T_1	Diesel (97%) – Gasoline (2%) – Sunflower Oil (1%)	3.190	0.8310
T_2	Diesel (90%) – Gasoline (5%) – Sunflower Oil (5%)	3.650	0.8335
T_3	Diesel (80%) – Gasoline (10%) – Sunflower Oil (10%)	4.050	0.8348
T_4	Diesel (70%) – Gasoline (15%) – Sunflower Oil (15%)	4.620	0.8365
T_5	Diesel (60%) – Gasoline (20%) – Sunflower Oil (20%)	5.310	0.8382
T_6	Diesel (50%) – Gasoline (25%) – Sunflower Oil (25%)	6.180	0.8399

Baseline density $\rho$and dynamic viscosity μvalues for all 13 biofuel formulations (N_1–N_7 and T_1–T_6) were established using a calibrated Anton Paar DMA 4100 M oscillating U-tube densimeter coupled with a Lovis 2000 M/ME rolling-ball viscometer. The reference system was calibrated using NIST-traceable APN10 standard oil and ultrapure deionized water. The resulting reference-measurement uncertainties were $\pm 1.0 \times 10^{-4}$ g/cm^{3}for density and $\pm 0.5\%$for dynamic viscosity. All reference measurements were performed in five independent replicates at a Peltier-controlled temperature of 25.00 ± 0.01°C. Because the flow-cell experiments were conducted under ambient conditions of 23.5 ± 1.5°C, the fluid temperature within the sensing cell was continuously monitored using an integrated temperature sensor. The measured temperature was incorporated into the auxiliary condition vector $z_t$and processed by the condition encoder $E_z(z_t)$. This condition-aware formulation enables the model to account for the temperature difference between ambient sensor operation and the controlled reference-measurement condition when estimating viscosity and density.

B. Broadband Spectral Acquisition

The sensor response arises from the coupled effects of inertial mass loading and viscous damping exerted by the liquid on the vibrating structure. Density primarily shifts the effective mass and therefore the resonance frequencies, while viscosity increases energy dissipation, broadening the resonances and reducing their amplitudes. Rather than relying on a single resonance parameter (frequency, quality factor, or amplitude), the system deliberately operates in broadband mode (40 kHz–1 MHz, 543 discrete frequency points). This captures the principal fourth-order mode together with the complementary (0,4), (0,5), and (0,6) modes and additional lower-amplitude spectral features.

The upper electrodes are arranged in an antiparallel configuration, realizing a true two-port actuator–detector architecture that allows simultaneous excitation and detection without the need for external directional couplers or complex impedance matching. Because liquid-induced changes are distributed across frequency, amplitude, and damping characteristics of multiple resonances, the complete spectral vector is retained as the primary input. No single-mode reduction or peak-tracking pre-processing is applied, thereby preserving the full information content available for subsequent adaptive learning.

This multi-resonance broadband strategy, combined with dual-side fluid access and optimized flow geometry, provides a richer and more robust sensing signature than conventional single-resonance piezoelectric densimeter-viscometers.

For each of the 15 fuel formulations, the liquid was introduced into the flow-through cell and allowed to undergo a 2-min stabilization period before spectral collection. The excitation frequency was swept continuously from 40 kHz to 1 MHz, yielding 543 discrete frequency points per spectrum. A total of 35 spectra were acquired for each formulation, corresponding to 315 spectra for the nine training formulations and 210 spectra for the six independent test formulations. Each spectrum was obtained by averaging 1000 measurements, with each measurement based on 10 signal periods, thereby reducing short-term measurement and electronic fluctuations. The same acquisition sequence was maintained across all fuel formulations to ensure consistency of the calibration and evaluation datasets.

The measured ADC spectrum at acquisition instant $t$is represented as

$$x^{(t)} = \left[x_1^{(t)}, x_2^{(t)}, \dots, x_{543}^{(t)}\right], \qquad (1)$$

where $x_i^{(t)}$denotes the measured detector amplitude at the i-th frequency point. Thus, the input dimension of the spectral branch is $N = 543$, covering the 40-kHz–1-MHz broadband sensing interval.

The acquired spectra are subjected to consistent preprocessing before model inference. Repeated measurements are averaged during acquisition, followed by spectral normalization using the training data. The same preprocessing transformation is subsequently applied to validation and test spectra to avoid information leakage. Because the proposed framework is designed to exploit multiresonance information, no individual resonance is used as the sole predictor.

C. Training, Validation, and Independent Testing

The seven binary diesel–sunflower-oil formulations N_1–N_7 comprising 315 spectra, constituted the model-development dataset. To prevent formulation-level data leakage, leave-one-formulation-out cross-validation (LOFO-CV) was used for model selection and hyperparameter optimization. The procedure consisted of seven folds, with all spectra from one formulation held out for validation and the spectra from the remaining six formulations used for training in each fold. Thus, spectra from the same formulation were never distributed between the training and validation subsets of a fold.

Spectral normalization and other data-dependent preprocessing operations were fitted exclusively using the training data within each fold and then applied unchanged to the corresponding validation data. Model selection and hyperparameter optimization were performed using the cross-validation results from N_1–N_7. After the model configuration was selected, the final model was retrained using the complete development dataset of 315 spectra, without an additional hold-out split. The final training duration was determined from the development-stage cross-validation procedure.

The six ternary diesel–gasoline–sunflower-oil formulations T_1–T_6were excluded from model fitting, preprocessing-parameter estimation, model selection, and hyperparameter optimization. These formulations were reserved for independent evaluation of generalization to previously unseen compositions. In particular, $T_1$and T_2 were used to assess responses to formulations containing relatively low gasoline and sunflower-oil fractions, whereas $T_3 - T_6$ assessed generalization across additional ternary compositions. After the final model was established, it was evaluated on the independent test set without further model adjustment.

This formulation-level validation strategy assesses generalization to an unseen formulation rather than merely to additional spectra from a formulation already represented in the training data.

D. Adaptive Condition-Aware Spectral Learning

The model processes a 543×1 spectral vector $\boldsymbol{x}_t$ alongside an auxiliary condition vector

$$\boldsymbol{c}_t = [T_t \quad \tau_t \quad r_t]^T,$$

where T_t denotes the fluid temperature (°C), τ_t denotes the operating time (h), and r_t denotes the baseline spectral shift.

The spectral encoder E_s is implemented as a three-layer one-dimensional convolutional neural network (1D-CNN), comprising Conv1D (32 filters, kernel size $k = 7$, stride $s = 2$, MaxPool1D (pool size $p = 2$, stride $s = 2$, Conv1D (64 filters, $k = 5$, $s = 1$ MaxPool1D (pool size $p = 2$, stride $s = 2$, Conv1D (128 filters, $k = 3$, $s = 1$, and global average pooling. The resulting representation is projected into a 64-dimensional spectral embedding, $\boldsymbol{h}_s \in \mathbb{R}^{64}$.

The condition encoder E_c maps $\boldsymbol{c}_t$ through a dense network with 3, 16, and 32 units, using Leaky ReLU activation with $\alpha = 0.2$, to produce a 32-dimensional condition embedding, $\boldsymbol{h}_z \in \mathbb{R}^{32}$.

Adaptive fusion F_{ada} is implemented using feature-wise linear modulation (FiLM). The fused representation is expressed as

$$\boxed{\boldsymbol{h}_f = \text{ReLU}[\boldsymbol{\gamma}(\boldsymbol{h}_z) \odot \boldsymbol{h}_s + \boldsymbol{\beta}(\boldsymbol{h}_z)]}$$

where $\boldsymbol{\gamma}(\cdot)$ and $\boldsymbol{\beta}(\cdot)$ generate 64-dimensional scale and shift vectors, respectively, from the condition embedding, and $\odot$.denotes element-wise multiplication. This condition-dependent modulation allows the spectral representation to adapt to the measured operating conditions and sensor state.

The finalized model, trained using the complete development dataset after model selection, was used for independent testing on T_1–T_6The independent test results were not used to adjust the model architecture, hyperparameters, preprocessing parameters, or training duration.

E. System Implementation and Training Protocol

The complete learning architecture contains 48,274 learnable parameters and is implemented using PyTorch v2.1.0. Following training, the model is converted and quantized for embedded deployment and executed directly on the ESP32 microcontroller, which handles broadband excitation, signal amplification, ADC sampling of the spectral vector xt, and on-device neural-network inference. Thus, the complete acquisition-to-prediction pipeline, including spectral encoding, adaptive fusion, and uncertainty estimation, is performed locally on the ESP32 hardware without reliance on an external host system.

The models are optimized using the Adam optimizer with $\beta_1 = 0.9$and $\beta_2 = 0.999$, using a batch size of 32 for a maximum of 200 epochs. The initial learning rate is set to $\eta_0 = 1.0 \times 10^{-3}$and decays according to a cosine-annealing schedule to a minimum learning rate of $\eta_{\min} = 1.0 \times 10^{-5}$. Early stopping is applied when the validation loss does not improve for 15 consecutive epochs.

Sensor-state tracking is performed over a 30-day monitoring period. At each monitoring instance, the spectral residual is computed relative to a baseline reference spectrum x_{ref}, acquired using pure diesel (N_1). The residual is then processed using a multilayer perceptron (MLP):

$$d_t = \text{MLP}(\|x_t - x_{\text{ref}}\|),$$

where $d_t$represents the learned sensor-state deviation relative to the baseline reference. The reference spectrum is retained as the baseline throughout the monitoring period, allowing temporal changes in the sensor response to be characterized without retraining the property-estimation model.

Model development uses the binary datasets N_1–N_7, comprising 315 spectra in total, with 252 spectra used for training and 63 spectra used for validation. The six independent ternary formulations T_1–T_6, comprising 210 spectra, are strictly excluded from model development and are used only for final out-of-sample evaluation.

F. Uncertainty-Aware Inference and Recalibration

The fused embedding $h_t$is supplied to two prediction branches. The Property Head consists of a 32-unit layer followed by a linear output layer and simultaneously predicts viscosity $\hat{\mu}$and density $\hat{\rho}$. The Uncertainty Head consists of a 16-unit layer followed by a Softplus activation and produces a strictly positive prediction variance $\sigma^2 > 0$.

The model is trained end-to-end using a heteroscedastic Gaussian negative log-likelihood (NLL) objective with L_2regularization:

$$\mathcal{L}_{\mathrm{NLL}} = \frac{1}{2N}\sum_{i=1}^{N}\left[\frac{\|y_i - \hat{y}_i\|^2}{\sigma_i^2} + \log(\sigma_i^2)\right] + \lambda \parallel \psi \parallel_2^2,$$

where $N$is the number of training samples, $y_i$and $\hat{y}_i$denote the reference and predicted property vectors, respectively, σ_i^2represents the predicted variance, $\lambda$is the L_2regularization coefficient, and ψdenotes the corresponding trainable parameters.

An automated recalibration request is triggered when the predicted uncertainty exceeds empirically determined thresholds, with $\sigma_{\mathrm{th}} = 0.045$mPa·s for viscosity and 6.0×10^{-4}g/mL for density. These thresholds are defined as three standard deviations above the corresponding validation-set mean uncertainty,

$$\sigma_{\mathrm{th}} = \mu_{\sigma,\mathrm{val}} + 3\sigma_{\sigma,\mathrm{val}},$$

where $\mu_{\sigma,\mathrm{val}}$and $\sigma_{\sigma,\mathrm{val}}$denote the mean and standard deviation of the validation uncertainty, respectively. When the predicted uncertainty exceeds the corresponding threshold, the measurement is flagged for reference verification and recalibration. The final evaluation is performed strictly out-of-sample using the six independent test formulations T_1–T_6, comprising 210 spectra that are not used during model training, validation, or hyperparameter selection..

RESULTS

The proposed system was evaluated using nine binary diesel–sunflower-oil blends for model development and six independent formulations, including low-concentration binary and previously unseen ternary mixtures. For each formulation, 35 broadband spectra with 543 frequency points were acquired over 40 kHz–1 MHz following a 2-min stabilization period, with each spectrum averaged over 1000 measurements.

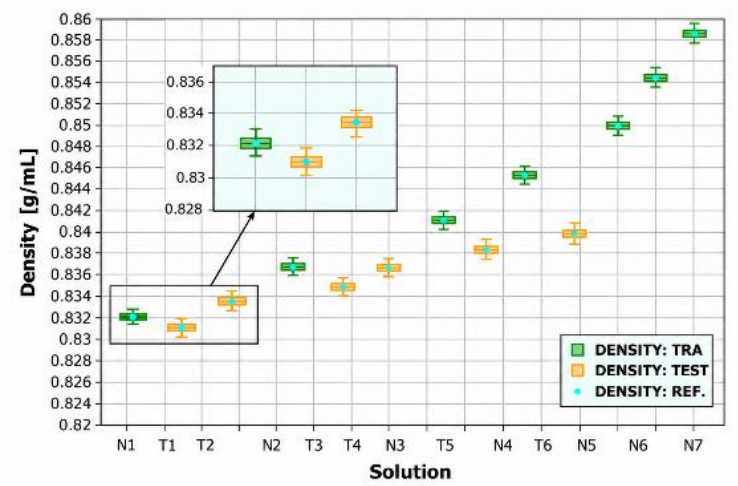


Fig. 3. Density estimation results for the investigated biofuel formulations.

The density estimates in Fig. 3 remain closely distributed around the reference values for both training and independent test formulations. The inset highlights the low-concentration region, demonstrating the sensor response to small changes in sunflower-oil content. The independent formulations further assess generalization beyond the calibration mixtures.

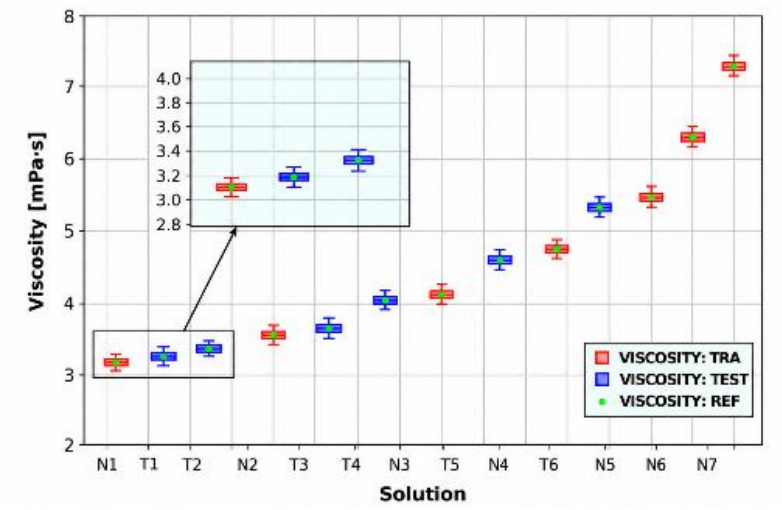


Fig. 4. Viscosity estimation results for the investigated biofuel formulations.

Fig. 4 shows the corresponding viscosity estimates, with the predicted distributions following the reference measurements across the investigated formulations. The magnified N1–T2 region illustrates the ability to distinguish small viscosity changes at low oil concentrations.

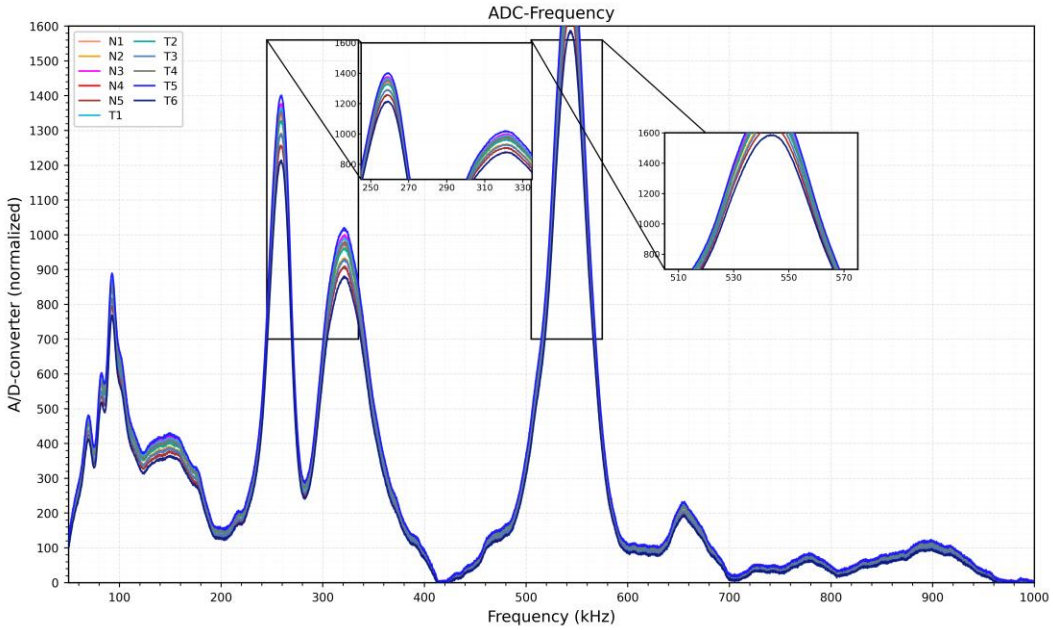


Fig. 5. Broadband ADC–frequency responses of the investigated biofuel formulations, with enlarged views of the principal resonance regions.

Fig. 5 exhibits prominent resonance features near **260, 320, and 545 kHz**. Fuel-composition changes produce measurable variations in resonance amplitude and spectral shape, supporting the use of the complete broadband response rather than a single resonance parameter. The acquired spectral vector spans 40 kHz–1 MHz with 543 frequency points.

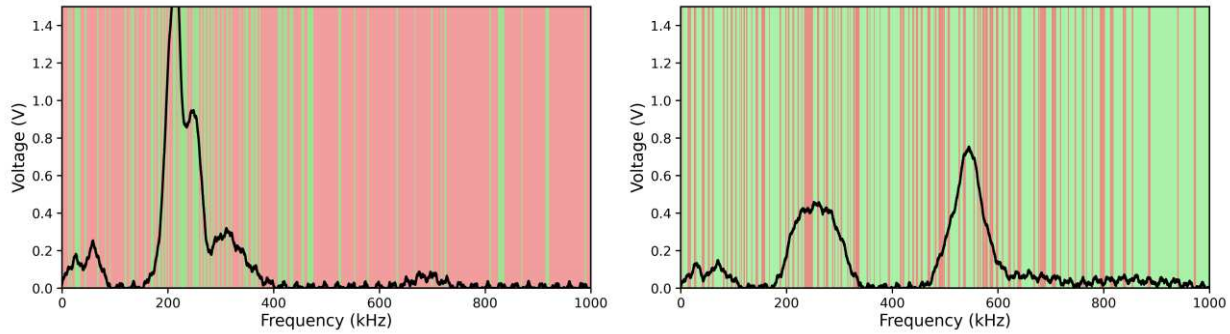


Fig. 6. Voltage–frequency responses illustrating composition-dependent variations in the resonant sensor output.

The voltage–frequency responses in Fig. 6 further show composition-dependent changes in resonance magnitude and spectral profile. These variations provide complementary information for the adaptive spectral-learning model.

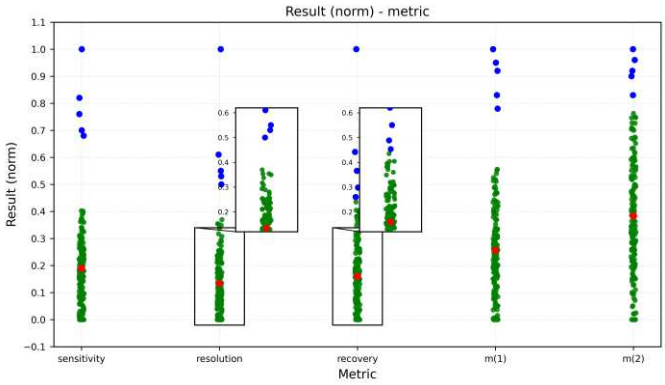


Fig. 7. Normalized sensor-performance metrics obtained from the experimental measurements.

Fig. 7 summarizes the normalized sensing characteristics, with sensitivity, resolution, and recovery values of approximately **0.19, 0.135, and 0.16**, respectively. The proposed framework incorporates temperature and reference-derived sensor-state information to account for operating and temporal variations. Reference-spectrum tracking was evaluated over a **30-day monitoring period**, while uncertainty-aware inference identifies measurements requiring reference verification or recalibration.

CONCLUSION

This paper presented a self-calibrating multiresonance piezoelectric MEMS sensor with adaptive learning for simultaneous biofuel viscosity and density monitoring. The proposed broadband approach preserves composition-dependent information across 40 kHz–1 MHz, including multiple dominant resonance features, while adaptive spectral fusion incorporates operating-condition and sensor-state information. Experimental evaluation using binary and independent ternary biofuel formulations demonstrated close agreement between predicted and reference viscosity and density values, including low-concentration and previously unseen mixtures. Reference-spectrum tracking and uncertainty-aware inference further provide a mechanism for identifying sensor-state deviations and supporting recalibration. These results demonstrate the feasibility of an intelligent and compact piezoelectric MEMS platform for robust biofuel property monitoring. Future work will focus on expanding the formulation and temperature range and validating long-term operation under controlled sensor drift and contamination conditions.

Funding Declaration

Funding: The authors received no financial support for the research, authorship, or publication of this article.

Declarations

Ethical approval : Not applicable.

Consent to participate : Not applicable.

Consent to publish : Not applicable.

Data Availability : The datasets generated and analysed during the current study will be made available by the corresponding author upon request after acceptance of the manuscript for publication.

References

[1 L. Razzaq et al., ‘Modeling viscosity and density of ethanol-diesel-biodiesel ternary blends for sustainable environment’, Sustainability, vol. 12, no. 12, p. 5186, 2020, doi: 10.3390/su12125186.

[2] R. Estevez et al., ‘Performance and emission quality assessment in a diesel engine of straight castor and sunflower vegetable oils, in diesel/gasoline/oil triple blends’, Energies, vol. 12, no. 11, p. 2181, 2019, doi: 10.3390/en12112181.

[3] T. Voglhuber-Brunnmaier, A. O. Niedermayer, F. Feichtinger, and B. Jakoby, ‘Fluid sensing using quartz tuning forks—Measurement technology and applications’, Sensors, vol. 19, no. 10, p. 2336, 2019, doi: 10.3390/s19102336.

[4] J. Toledo et al., ‘Application of quartz tuning forks and extensional microresonators for viscosity and density measurements in oil/fuel mixtures’, Microsystem technologies, vol. 20, no. 4, pp. 945–953, 2014, doi: 10.1007/s00542-014-2095-x.

[5] J. Toledo, V. Ruiz-Díez, G. Pfusterschmied, U. Schmid, and J. L. Sánchez-Rojas, ‘Characterization of oscillator circuits for monitoring the density-viscosity of liquids by means of piezoelectric MEMS microresonators’, in Smart Sensors, Actuators, and MEMS VIII, 2017, vol. 10246, pp. 380–390, doi: 10.1117/12.2266497.

[6] J. Toledo et al., ‘Comparison of in-plane and out-of-plane piezoelectric microresonators for real-time monitoring of engine oil contamination with diesel’, Microsystem Technologies, vol. 22, no. 7, pp. 1781–1790, 2016, doi: 10.1007/s00542-016-2833-3.

[7] G. Pfusterschmied et al., ‘Temperature dependent performance of piezoelectric MEMS resonators for viscosity and density determination of liquids’, Journal of Micromechanics and Microengineering, vol. 25, no. 10, p. 105014, 2015, doi: 10.1088/0960-1317/25/10/105014.

[8] M. Ghaderi, B. Jiang, A. Bossche, J. H. Visser, and R. F. Wolffenbuttel, “MEMS for biofuel composition measurement based on thermal impedance spectroscopy,” *Sensors and Actuators B: Chemical*, vol. 277, pp. 281–288, 2018, doi: 10.1016/j.snb.2018.08.098.

[9] S. Goel, P. S. Venkateswaran, R. Prajesh, and A. Agarwal, “Rapid and automated measurement of biofuel blending using a microfluidic viscometer,” *Fuel*, vol. 139, pp. 213–219, 2015, doi: 10.1016/j.fuel.2014.08.053.

[10] J. L. Camas-Anzueto et al., "Measurement of the viscosity of biodiesel by using an optical viscometer," Flow Measurement and Instrumentation, vol. 54, pp. 82–87, 2017, doi: 10.1016/j.flowmeasinst.2016.12.004.

[11] M. Baghelani, N. Hosseini, and M. Daneshmand, "Artificial intelligence assisted noncontact microwave sensor for multivariable biofuel analysis," IEEE Trans. Ind. Electron., vol. 68, no. 11, pp. 11492–11500, 2021, doi: 10.1109/TIE.2020.3032870.

[12] A. Urban and J. Zhe, "A microsensor array for diesel engine lubricant monitoring using deep learning with stochastic global optimization," Sensors and Actuators A: Physical, vol. 343, Art. no. 113671, 2022, doi: 10.1016/j.sna.2022.113671.

[13] A. Moradkhani, O. Hasannejad, and M. Baghelani, "An artificial intelligence assisted distance variation robust microwave sensor for biofuel analysis applications," IEEE Microw. Wirel. Compon. Lett., vol. 32, no. 12, pp. 1475–1478, 2022, doi: 10.1109/LMWC.2022.3177403.

[14] V. Corsino, V. Ruiz-Díez, and J. L. Sánchez-Rojas, "Innovative sensor systems using deep learning and piezoelectric resonators for biofuel monitoring," IEEE Sensors Papers, vol. 9, Art. no. 5502804, 2025, doi: 10.1109/LSENS.2025.3587851.

[15] T. P. Vello, R. F. de Oliveira, G. O. Silva, D. H. de Camargo, and C. C. Bufon, "A simple capacitive method to evaluate ethanol fuel samples," Scientific Reports, vol. 7, no. 1, Art. no. 43432, 2017, doi: 10.1038/srep43432.

[16] J. Toledo, V. Ruiz-Díez, G. Pfusterschmied, U. Schmid, and J. L. Sánchez-Rojas, "Calibration procedure for piezoelectric MEMS resonators to determine simultaneously density and viscosity of liquids," Microsyst. Technol., 2018, doi: 10.1007/s00542-017-3536-0.

[17] J. Toledo et al., "Piezoelectric MEMS resonators for density and viscosity sensing in engine oil with diesel fuel," in Proc. Transducers 2015, doi: 10.1109/TRANSDUCERS.2015.7180954.

[18] J. Toledo, V. Ruiz-Díez, J. Velasco, J. Hernando-García, and J. L. Sánchez-Rojas, "3D-printed liquid cell resonator with piezoelectric actuation for in-line density-viscosity measurements," Sensors, vol. 21, no. 22, Art. no. 7654, 2021, doi: 10.3390/s21227654.

[19] V. Corsino, V. Ruiz-Díez, M. Ramírez-Palma, J. Toledo, J. M. Gilpérez, and J. L. Sánchez-Rojas, "Three-dimensionally printed resonator with piezoelectric actuation and machine learning calibration for in-line density-viscosity sensing," Proceedings, vol. 97, no. 1, p. 55, 2024, doi: 10.3390/proceedings2024097055.

[20] A. Cowen, G. Hames, D. Monk, S. Wilcenski, and B. Hardy, PiezoMUMPs Design Handbook, MEMSCAP Inc.

[21] A. Vergara, S. Vembu, T. Ayhan, M. A. Ryan, M. L. Homer, and R. Huerta, "Chemical gas sensor drift compensation using classifier ensembles," Sens. Actuators B, Chem., vol. 166–167, pp. 320–329, 2012, doi: 10.1016/j.snb.2012.01.074.

[22] H. Liu and Z. Tang, "Metal oxide gas sensor drift compensation using a two-dimensional classifier ensemble," Sensors, vol. 15, no. 5, pp. 10180–10193, 2015, doi: 10.3390/s150510180.

[23] E. Perez, F. Strub, H. de Vries, V. Dumoulin, and A. Courville, "FiLM: Visual reasoning with a general conditioning layer," in Proc. AAAI Conf. Artif. Intell., 2018, pp. 3942–3951.

[24] D. A. Nix and A. S. Weigend, "Estimating the mean and variance of the target probability distribution," in Proc. IEEE Int. Conf. Neural Netw., 1994, vol. 1, pp. 55–60.

[25] A. Kendall and Y. Gal, "What uncertainties do we need in Bayesian deep learning for computer vision?," in Proc. Adv. Neural Inf. Process. Syst., 2017, pp. 5574–5584.

[26] B. Lakshminarayanan, A. Pritzel, and C. Blundell, "Simple and scalable predictive uncertainty estimation using deep ensembles," in Proc. Adv. Neural Inf. Process. Syst., 2017, pp. 6402–6413.

[27] C. Guo, G. Pleiss, Y. Sun, and K. Q. Weinberger, "On calibration of modern neural networks," in Proc. Int. Conf. Mach. Learn., 2017, pp. 1321–1330.

[28] Y. Ovadia et al., "Can you trust your model's uncertainty? Evaluating predictive uncertainty under dataset shift," in Proc. Adv. Neural Inf. Process. Syst., 2019, pp. 13991–14002.

[29] B. Jacob et al., "Quantization and training of neural networks for efficient integer-arithmetic-only inference," in Proc. IEEE Conf. Comput. Vis. Pattern Recognit., 2018, pp. 2704–2713.

[30] R. David et al., "TensorFlow Lite Micro: Embedded machine learning for TinyML systems," in Proc. Mach. Learn. Syst., vol. 3, 2021, pp. 800–811